Blob Transport in the Plasma Edge: a Review*)

O. E. GARCIA

Department of Physics and Technology, University of Tromsø, N-9037 Tromsø, Norway

(Received 3 September 2008 / Accepted 13 March 2009)

A brief review is presented of transport in the boundary region of magnetized plasmas by blob-like filaments. Such structures have enhanced levels of particles and heat, are elongated along the magnetic field lines and are localized in the drift plane across the field. The motion of an isolated blob structure is described in some detail and the contribution of such filaments to turbulence-driven transport are discussed. Results are presented from numerical simulations and probe measurements in tokamak plasmas. An interpretation is given of the measured dependence of particle density and transport on experimental control parameters in the scrape-off layer.

Keywords: blob, filament, turbulence, transport, scrape-off layer

DOI: 10.1585/pfr.4.019

1. Introduction

The boundary region of magnetically confined plasmas has been known to have inherently fluctuating parameters ever since the first probe measurements were made [1–5]. Until recently, the nature of these fluctuations remained a puzzle. This was particularly so in the outermost region with magnetic field lines intersecting material walls, known as the scrape-off layer. However, major advances in experimental measurements and theoretical modelling have revealed that fluctuation-driven transport across the magnetic field lines is largely dominated by the radial motion of filamentary structures which are localized in the drift plane perpendicular to the field and elongated along the field lines. These filaments contain excess particles and heat compared to the background plasma, and are thus referred to as plasma blobs [6–15].

The radial motion of blob-like structures in the scrape-off layer of magnetically confined plasmas causes large cross-field transport of particles and heat and may strongly influence the properties of the scrape-off layer and divertor operation. In particular, the fluctuation-driven transport lead to a broadening of the radial plasma profile and thereby erosion of the main chamber walls. The transport mediated by such blob structures is likely related to a number of outstanding problems for the steady operation of a fusion experiment, including main chamber recycling, material migration, plasma rotation and the density disruption limit [16–20].

The dynamics of blob-like structures and the associated fluctuation-induced radial transport have been the subject of several recent reviews [6–10]. This paper will therefore mostly emphasize those issues that have not been considered in these previous reports. In the following section, the dynamics of an isolated blob structure is considered [11–15]. The mechanism for radial motion is elucidated and an inertial velocity scaling in the absence of dissipation and parallel currents is derived. A discussion of the dynamics of isolated blob structures in numerical simulations and basic laboratory experiments is also presented in Sec. 2.

Fluctuations and turbulence-driven transport in the scrape-off layer of magnetically confined plasmas are considered in Sec. 3. Probe measurements of the particle density in the outboard mid-plane region reveal large fluctuation levels and an abundance of bursts in the time series that correspond to blob-like structures [21–25]. For a large variation in the experimental control parameters, the fluctuations are found to exhibit universal probability distributions and temporal correlations, which indicates that the same physical mechanism underlies the fluctuations in all parameter regimes [26–31].

However, it is also found that the time-average particle density at the wall radius increases as the square of the line-averaged plasma density and inversely with the plasma current [30–32]. This indicates a strong dependence on plasma collisionality, as is also found from turbulence simulations of the plasma edge region with closed magnetic surfaces. In Sec. 3 a discussion is given of the observed parameter dependence and its relation to blob motion. Finally, a discussion of the results and conclusions are presented in Sec. 4.

2. Isolated Blobs

Consider an isolated blob-like structure initially at rest, which is elongated along the magnetic field and localized in the drift plane perpendicular to the field lines. An illustration of such a structure is given in Fig. 1. If the magnetic field is non-uniform, guiding center drifts caused by magnetic field gradient and curvature causes an electric

author's e-mail: odd.erik.garcia@uit.no

*) This article is based on the invited talk at the 14th International Congress on Plasma Physics (ICPP2008).

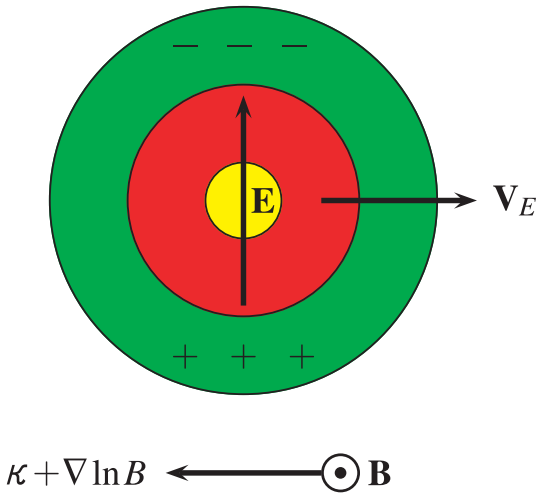

Fig. 1 An isolated blob structure with positive pressure perturbation $\widetilde{P} > 0$ which is localized in the drift plane perpendicular to a non-uniform magnetic field.

current density given by

$$\boldsymbol{J}_B = \frac{P}{B}\,\boldsymbol{b} \times (\boldsymbol{\kappa} + \nabla \ln B)\,, \tag{1}$$

where $\boldsymbol{b}$ is a unit vector along the magnetic field, P the plasma pressure and $\boldsymbol{\kappa} = (\boldsymbol{b}\cdot\nabla)\boldsymbol{b}$ the magnetic field curvature vector. For a structure with excess pressure compared to the background plasma, this results in a vertical charge polarization within the filament and a radial electric drift at the center of the blob structure [13–15].

Taking into account polarization currents due to plasma inertia, the charge continuity equation for low-frequency variations is given by

$$\nabla\cdot\left(\frac{\rho_{\rm m}}{B}\frac{\mathrm{d}}{\mathrm{d}t}\frac{\nabla_\perp\phi}{B}\right) + \frac{1}{B}\,\boldsymbol{b}\times(\boldsymbol{\kappa} + \nabla \ln B)\cdot\nabla P = \nabla\cdot\boldsymbol{J}_{\shortparallel}, \tag{2}$$

where $\rho_{\rm m}$ is the plasma mass density, ϕ the electrostatic potential, and $\boldsymbol{J}_{\shortparallel}$ the current density along the field lines. The left hand side of the above equation predicts an inertial blob velocity scaling [13, 14]

$$\frac{C_{\rm b}}{C_{\rm s}} \sim \left(\frac{2\ell}{R}\frac{\triangle P}{\Pi}\right)^{1/2}, \tag{3}$$

where $C_{\rm s} = (\Pi/\rho_{\rm m})$ is the acoustic speed, Π the background plasma pressure, $\triangle P$ is the blob pressure amplitude, R the magnetic field radius of curvature and ℓ the initial structure size across field lines. Thus, the larger the blob structure, in either size or amplitude, the larger the radial velocity it develops. An analysis of the size, amplitude and velocity of several hundred edge localized mode filaments from probe measurements in the scrape-off layer of the ASDEX tokamak have revealed a scaling consistent with this theoretical prediction [33].

A two-field model for the plasma pressure and vorticity has been solved numerically to reveal the evolution

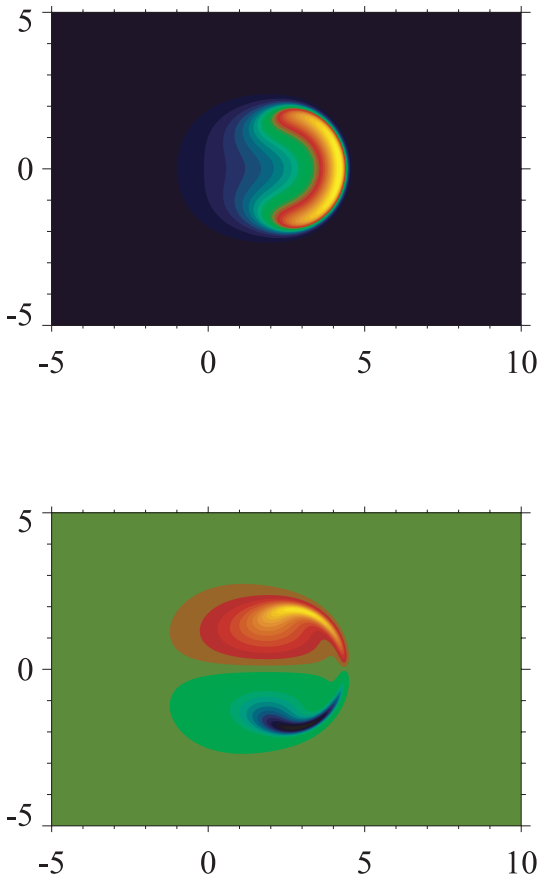

Fig. 2 Plasma pressure (top) and vorticity (bottom) after five ideal interchange time units, starting with a Gaussian shaped blob initially at rest at the origin of the coordinate system. Length scales are normalized to the initial blob size ℓ. The horizontal and vertical axes correspond to the normalized radial (x) and poloidal (y) coordinates, respectively.

and motion of a plasma blob structure initially at rest and with a Gaussian pressure distribution [13–15]. As shown in Fig. 2, the vertical charge separation leads to a radial electric drift at the center of the blob structure. The characteristic time scale is given by the ideal interchange rate $\gamma = (g\triangle P/\ell\Pi)^{1/2}$, where $g = C_{\rm s}^2/R$ is the effective gravity due to the non-uniform magnetic field. After a few ideal interchange times, the blob structure has moved a radial distance several times the initial structure size. During this initial acceleration, the structure develops an asymmetric wave form with a steep front and a trailing wake as is clearly seen in Fig. 3. A similar structure and dynamical evolution of toroidally symmetric plasma blobs have been found from probe measurements in the simply magnetized torus experiment VTF [34].

Parallel currents may severely influence the radial motion of blob-like structures. Several idealized cases can be considered. For two-dimensional structures which are perfectly aligned with the magnetic field, currents through electrostatic sheaths where the field lines intersect mate-

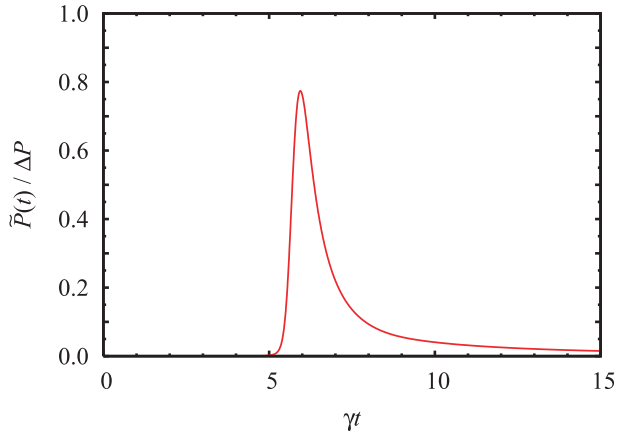

Fig. 3 Probe recording of a blob structure at a radial distance of five times the initial blob size, showing the development of a steep front and a trailing wake.

rial walls cause sheath dissipation of large perpendicular scale lengths, $\langle \nabla \cdot \boldsymbol{J}_{\shortparallel} \rangle \sim (C_s/L_{\shortparallel}) \langle \phi \rangle$, where $L_{\shortparallel}$ is the magnetic connection length [10–13]. Numerical simulations of an isolated blob structure have shown that the maximum radial center of mass velocity gradually decreases with increasing sheath dissipation coefficient [13]. However, if the structure has a finite correlation along the field lines, outgoing Alfvén waves result in an effective friction, $\langle \nabla \cdot \boldsymbol{J}_{\shortparallel} \rangle \sim (C_A/L_{\shortparallel}) \nabla_{\perp}^2 \langle \phi \rangle$, where $L_{\shortparallel}$ is now the parallel structure length [35, 36]. Finally, for strongly collisional plasmas we may expect the parallel current to be given by the resistive Ohm's law, $\boldsymbol{J}_{\shortparallel} = \eta \boldsymbol{E}_{\shortparallel}$. The contribution to the vorticity equation then gives a parallel diffusion term for the electrostatic potential.

Due to unfavorable magnetic curvature, fluctuation levels and turbulence-driven particle and heat transport in tokamak plasmas are poloidally asymmetric with peak values in the outboard mid-plane region. This ballooning structure of the fluctuations has been clearly demonstrated by experimental measurements [37–41]. It is therefore plausible that the plasma filaments themselves have a ballooning structure. The associated pressure gradient along the field lines would then drive parallel flows in the scrape-off layer, which have been demonstrated experimentally [39–43]. Ballooning combined with high resistivity may diminish the effect of sheath currents at material walls in the scrape-off layer. As a result of reduced sheath dissipation, higher radial velocities of the blob structures are expected. However, the many possible influences of parallel currents call for an analysis of isolated blob structures using three-dimensional models which include Alfvén waves, resistivity, sheath boundary conditions in the parallel direction and allowing for order unity perturbations to the background parameters. Such investigations are now in progress using both slab and flux tube geometry.

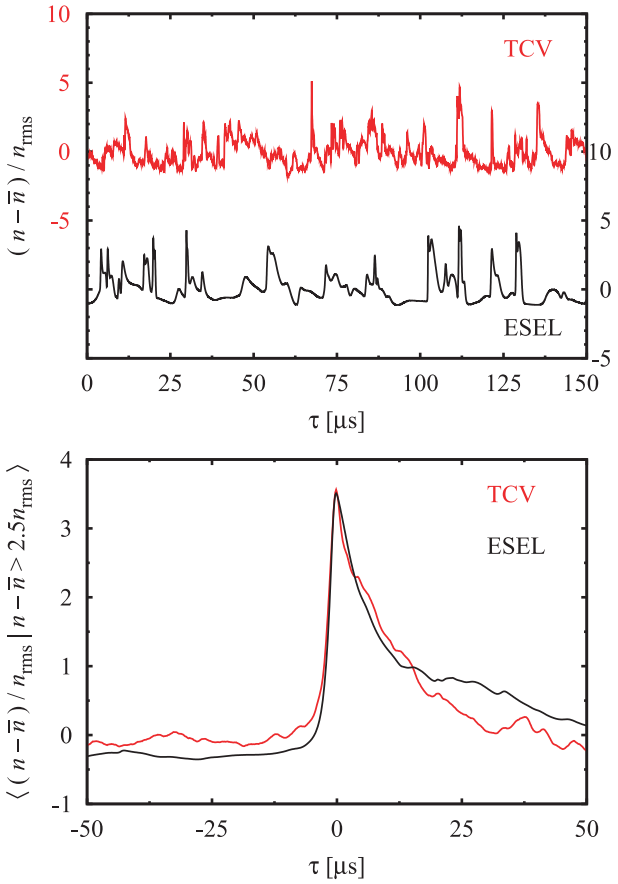

Fig. 4 Probe recording (top) of the particle density and its conditional average (bottom) in the TCV scrape-off layer and in a two-dimensional interchange turbulence simulation (ESEL).

3. Turbulence and Transport

Plasma parameters in the scrape-off layer of magnetic confinement experiments are characterized by large relative fluctuation levels. As an example, Fig. 4 shows the particle density signal at the wall radius in the outboard mid-plane region of the TCV scrape-off layer [29, 30]. There is an abundance of large amplitude bursts in the time series which appear to have an asymmetric wave form. This is clearly demonstrated by conditional averaging of these events, which reveals a steep front and a trailing wake. The typical duration of one burst event is in excess of 25 μs and the amplitude is more than four times the rms value of the particle density fluctuations. These bursts in the probe time series are associated with blob structures. Fast camera gas puff imaging on other tokamaks has clearly demonstrated their filamentary structure and radial motion in the scrape-off layer [44–47].

Also presented in Fig. 4 is a time series of the particle density taken from a simple two-dimensional turbulence simulation which models the evolution of plasma pressure and vorticity in the scrape-off layer [48–50]. Important features of these simulations are the separation of the simulation domain into an edge region corresponding

to closed magnetic surfaces ($\rho < 0$) and scrape-off layer ($0 < \rho < 1$) and wall shadow regions ($\rho > 1$) with strong damping of all dependent variables to account for transport along field lines intersecting material walls. All profiles evolve self-consistently with order unity fluctuation levels. Time series of the plasma parameters at fixed radial positions are recorded and analyzed similar to the experimental data [48–50].

For a large range of model parameters, the numerical simulations show intermittent eruptions of plasma and heat into the scrape-off layer. An example of the structures observed in these simulations is presented in Fig. 5. Associated with the blob structures are large amplitude bursts in the probe time series, as shown in Fig. 4. These were the first simulations to reproduce the salient experimental observations and a detailed comparison with probe measurements on TCV showed excellent agreement for the temporal correlations and statistical distribution of the particle density and turbulence-driven transport in the scrape-off layer [28–30].

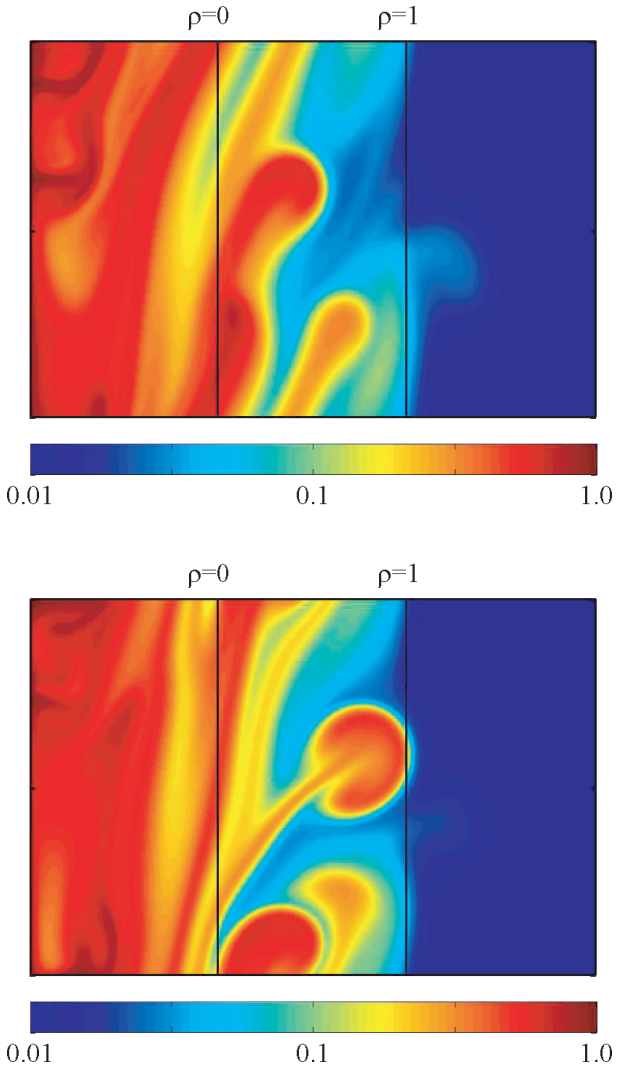

Fig. 5 Motion of blob-like structures in the particle density from two-dimensional turbulence simulations. The vertical line labeled $\rho = 0$ corresponds to the last closed flux surface while the line labeled $\rho = 1$ corresponds to the wall radius. The bottom panel follows a time $30/\omega_{ci}$ after the top panel, where $\omega_{ci} = eB/m_i$ is the ion gyration frequency. The size of the simulation domain is $150\,\rho_s$ in the radial direction (horizontal axis) and $100\,\rho_s$ in the poloidal direction (vertical axis), where $\rho_s = C_s/\omega_{ci}$.

Probe measurements in the TCV scrape-off layer demonstrate that the fluctuations have universal properties for a large variation in experimental control parameters [26–31]. This is clearly demonstrated in Figs. 6 and 7, which show the rescaled conditional averages and probability distribution functions of the particle density for a scan in line-averaged density ($\overline{n}_e$ measured in $10^{19}\,m^{-3}$) and plasma current (I_p measured in kA). The probability distribution functions of the particle density signals are positively skewed and flattened due to the many large-amplitude bursts in the time series. When appropriately rescaled, the conditional averages and distribution functions have similar shapes across both the density and current scans. This strongly suggests that the same physical mechanism underlies the fluctuations in all these parameter regimes.

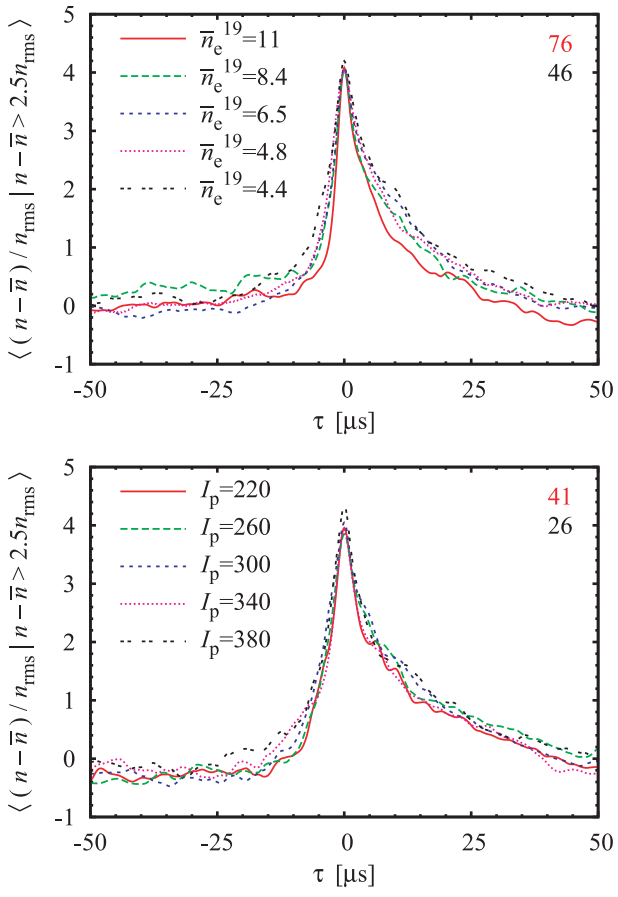

Fig. 6 Conditionally averaged particle density fluctuations in TCV scrape-off layer for a scan in line-averaged density and plasma current.

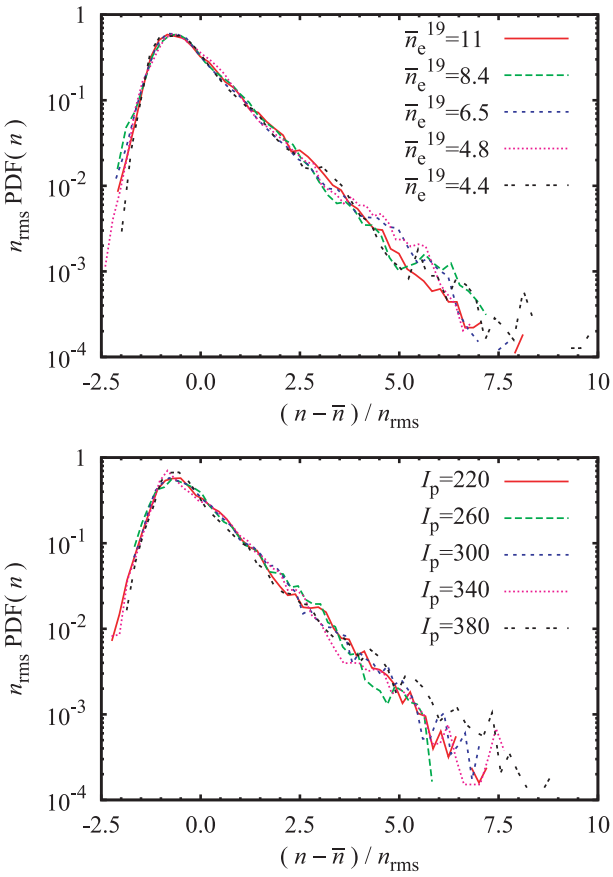

Fig. 7 Rescaled probability distribution functions of the particle density fluctuations in TCV scrape-off layer for a scan in line-averaged density and plasma current.

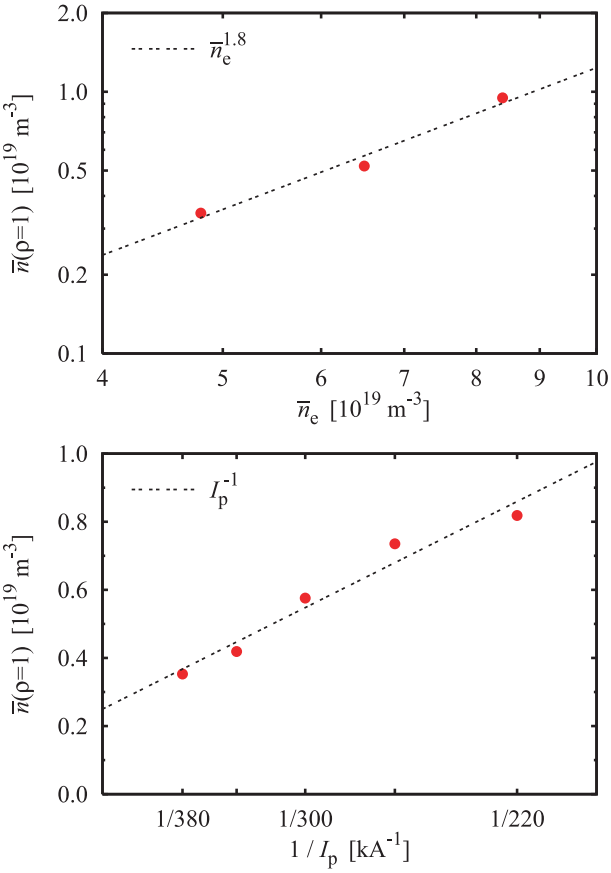

Fig. 8 Time-averaged particle density at the wall radius as function of line-averaged density and plasma current in TCV.

While the fluctuations display universal statistics, the absolute fluctuation level and time-averaged values of the particle density and radial turbulence-driven particle flux in the scrape-off layer change markedly with experimental control parameters [28, 30, 31]. In Fig. 8 the measured time-averaged particle density at the wall radius in TCV is presented as function of line-averaged density and plasma current. It is seen that the local density scales as the square of the line-averaged density and inversely with the plasma current. A similar dependence on the line-averaged density has been found from measurements on several other tokamak experiments [32].

As the line-averaged density increases from $4.4 \times 10^{19}\,m^{-3}$ to $11 \times 10^{19}\,m^{-3}$ in the TCV density scan, the number of conditional events for a fixed time series duration of 1 ms increases from 46 to 76. For the current scan experiments, the number of conditional events increases from 26 at the highest current of 380 kA to 41 events at the lowest current of 220 kA. The associated increase in blob transport evidently contribute to the enhanced plasma density in the far scrape-off layer.

The radial fluctuation driven-particle transport in the TCV experiments has been estimated from measurements of the probe saturation current and the floating potential by two probe pins separated vertically by 10 mm. A calculation of the time-averaged particle flux at the wall radius reveals a scaling with the line-averaged density and plasma current which is nearly identical to that of the local particle density presented above. This result implies that the turbulence driven particle flux is proportional to the particle density, with the proportionality constant being an effective convection velocity. This shows that the conventional flux-gradient paradigm is clearly not valid for fluctuation-driven transport in the far scrape-off layer [7, 28].

4. Discussion and Conclusions

Numerical simulations of plasma edge turbulence in flux-tube geometry have revealed a substantial increase in the particle and heat transport with increasing plasma beta and collisionality [9, 51–53]. This is consistent with the increase of transport with average density in global fluid turbulence simulations which comprises both the edge region with closed magnetic surfaces and a scrape-off layer [54]. Moreover, recent flux-tube simulations which include a scrape-off layer region also reveal radial motion of plasma blobs [55, 56]. By altering the boundary conditions in the parallel direction in these simulations, it has been found that turbulence driven transport is strongly reduced with

sheath boundary conditions compared to periodic or fixed flux conditions.

Putting together the pieces of the puzzle outlined above, an understanding of the parameter dependence of fluctuations and turbulence-driven transport in the boundary region of magnetically confined plasmas emerges. Given that blob-like structures are generated from the prevalent edge plasma turbulence, the structures appearing in the scrape-off layer will have large relative fluctuation amplitudes. If the structures are ballooned, the interchange mechanism causes a radially outwards motion at the outboard mid-plane region. This may result in strong cross-field transport and a broadening of the radial particle density profile in the scrape-off layer.

Since the edge turbulence and radial transport levels increase with plasma beta and collisionality, one would also expect a similar increase in the occurrence of blob structures in the scrape-off layer. This is consistent with the measured increase in the particle density and flux at the wall radius and the reduction in waiting time between large-amplitude events in the particle density time series with increasing line-averaged density and decreasing plasma current, as reported in the previous section. Stronger turbulence in the edge plasma region naturally causes more transport of particles and heat into the scrape-off layer.

The radial velocity associated with blob structures in the scrape-off layer can be estimated by a cross-conditional average of the particle density and electrostatic potential signals. In the TCV current scan experiments, it was found that the estimated radial blob velocity increases with decreasing plasma current [31]. Moreover, the rms value of the radial velocity in the far scrape-off layer increases with increasing line-averaged density and decreasing plasma current. In this limit there are more blob structures present and they move faster, thereby increasing the radial particle flux and average particle density in the scrape-off layer.

Since plasma collisionality scales linearly with the particle density and inversely with the plasma current, the measured parameter dependence is consistent with an increase of fluctuation levels and turbulence-driven transport with plasma collisionality in the scrape-off layer. Due to ballooning and increased resistivity, this might effectively prevent electrical connection of the filamentary structures with the electrostatic sheaths where the magnetic field intersects material walls. The associated reduction in sheath dissipation would expectedly lead to a larger radial velocity of the blob structures, as observed in the experiments. These mechanisms might play a fundamental role in the density disruption limit.

Transport in the boundary region of magnetically confined plasmas has for a long time remained a puzzle. Many previous efforts attempted to understand the anomalously large transport and its parameter dependence based on the flux-gradient paradigm, according to which linear instabilities and the resulting turbulence-driven transport are driven by local profile gradients in the scrape-off layer. Recent advances in experimental measurements and theoretical modelling have revealed that the radial transport is largely mediated by radial motion of filamentary structures which appear as blobs of excess particle and heat in the drift plane perpendicular to the magnetic field. The resulting radial particle and heat transport likely underlies a number of phenomena of importance to future fusion experiments, including main chamber recycling, particle migration, plasma rotation and the density disruption limit.

[1] C.M. Surko and R.E. Slusher, Science **221**, 817 (1983).
[2] A.V. Nedospasov, J. Nucl. Mater. **196–198**, 90 (1982).
[3] P.C. Liewer, Nucl. Fusion **25**, 543 (1985).
[4] A.J. Wootton *et al.*, Phys. Fluids B **2**, 2879 (1990).
[5] F. Wagner and U. Stroth, Plasma Phys. Control. Fusion **35**, 1321 (1993).
[6] M. Endler, J. Nucl. Mater. **266–269**, 84 (1999).
[7] V. Naulin, J. Nucl. Mater. **363–365**, 24 (2007).
[8] S. Zweben *et al.*, Plasma Phys. Control. Fusion **49**, S1 (2007).
[9] B. Scott, Plasma Phys. Control. Fusion **49**, S25 (2007).
[10] S.I. Krasheninnikov, D.A. D'Ippolito and J.R. Myra, J. Plasma Phys. **74**, 679 (2008).
[11] S.I. Krasheninnikov, Phys. Lett. A **283**, 368 (2001).
[12] D.A. D'Ippolito *et al.*, Contrib. Plasma Phys. **44**, 205 (2004).
[13] O.E. Garcia *et al.*, Phys. Plasmas **13**, 082309 (2006).
[14] O.E. Garcia *et al.*, Phys. Plasmas **12**, 090701 (2005).
[15] N.H. Bian *et al.*, Phys. Plasmas **10**, 671 (2003).
[16] B. LaBombard *et al.*, Phys. Plasma **8**, 2107 (2001).
[17] B. Lipschultz *et al.*, Plasma Phys. Control. Fusion **47**, 1559 (2005).
[18] D.G. Whyte *et al.*, Plasma Phys. Control. Fusion **47**, 1579 (2005).
[19] R.A. Pitts *et al.*, Plasma Phys. Control. Fusion **47**, B303 (2005).
[20] B. LaBombard *et al.*, Nucl. Fusion **45**, 1658 (2005).
[21] J.A. Boedo *et al.*, Phys. Plasmas **8**, 4826 (2001).
[22] G.Y. Antar *et al.*, Phys. Rev. Lett. **87**, 065001 (2001).
[23] J.A. Boedo *et al.*, Phys. Plasmas **10**, 1670 (2003).
[24] G.Y. Antar *et al.*, Phys. Plasmas **10**, 419 (2003).
[25] D.L. Rudakov *et al.*, Nucl. Fusion **45**, 1589 (2005).
[26] J.P. Graves *et al.*, Plasma Phys. Control. Fusion **47**, L1 (2005).
[27] J. Horacek *et al.*, Czech. J. Phys. **55**, 271 (2005).
[28] O.E. Garcia *et al.*, J. Nucl. Mater. **363–365**, 575 (2007).
[29] O.E. Garcia *et al.*, Plasma Phys. Control. Fusion **48**, L1 (2006).
[30] O.E. Garcia *et al.*, Nucl. Fusion **47**, 667 (2007).
[31] O.E. Garcia *et al.*, Plasma Phys. Control. Fusion **49**, B49 (2007).
[32] B. LaBombard *et al.*, Cross-field transport in the SOL: its relationship to main chamber and divertor neutral control in Alcator C-Mod, Proc. 18th Int. Conf. on Fusion Energy 2000 (Sorrento, 2000) (Vienna: IAEA) CD-ROM file EX5/6.
[33] A. Schmid *et al.*, Plasma Phys. Control. Fusion **50**, 045007 (2008).
[34] N. Katz *et al.*, Phys. Rev. Lett. **101**, 0153004 (2008).
[35] V. Rozhansky *et al.*, Plasma Phys. Control. Fusion **37**, 399 (1995).

[36] P.B. Parks *et al.*, Phys. Plasmas **7**, 1968 (2000).
[37] J.L. Terry *et al.*, Phys. Plasmas **10**, 1739 (2001).
[38] N. Smick *et al.*, J. Nucl. Mater. **337–339**, 281 (2005).
[39] B. LaBombard *et al.*, Nucl. Fusion **44**, 1047 (2004).
[40] B. LaBombard *et al.*, Phys. Plasmas **12**, 056111 (2005).
[41] J. Gunn *et al.*, J. Nucl. Mater. **363–365**, 484 (2007).
[42] S.K. Erents *et al.*, Plasma Phys. Control. Fusion **46**, 1757 (2004).
[43] R.A. Pitts *et al.*, J. Nucl. Mater. **363–365**, 505 (2007).
[44] S.J. Zweben *et al.*, Phys. Plasmas **9**, 1981 (2002).
[45] S.J. Zweben *et al.*, Nucl. Fusion **44**, 134 (2004).
[46] J.L. Terry *et al.*, Nucl. Fusion **45**, 1321 (2005).
[47] O. Grulke *et al.*, Phys. Plasmas **13**, 012306 (2006).
[48] O.E. Garcia *et al.*, Phys. Rev. Lett. **92**, 165003 (2004).
[49] O.E. Garcia *et al.*, Phys. Plasmas **12**, 062309 (2005).
[50] O.E. Garcia *et al.*, Phys. Scripta **T122**, 089 (2006).
[51] B.N. Rogers *et al.*, Phys. Rev. Lett. **81**, 4396 (2000).
[52] V. Naulin *et al.*, Phys. Plasmas **10**, 4016 (2005).
[53] R. Kleva *et al.*, Phys. Plasmas **15**, 082307 (2008).
[54] X.Q. Xu *et al.*, Phys. Plasmas **10**, 1773 (2003).
[55] T. Ribeiro and B.D. Scott, Plasma Phys. Control. Fusion **47**, 1657 (2005).
[56] T. Ribeiro and B.D. Scott, Plasma Phys. Control. Fusion **50**, 055007 (2008).